American Mineralogist, Volume 90, pages 653–662, 2005

Crystal chemistry of the hydrothermally synthesized $Na_2(Mn_{1-x}Fe^{2+}_x)_2Fe^{3+}(PO_4)_3$ alluaudite-type solid solution

FRÉDÉRIC HATERT,[1,2,*] LEILA REBBOUH,[3] RAPHAËL P. HERMANN,[3] ANDRÉ-MATHIEU FRANSOLET,[1] GARY J. LONG,[4] AND FERNANDE GRANDJEAN[3]

[1]Laboratoire de Minéralogie, B18, Université de Liège, B-4000 Sart-Tilman, Belgium
[2]Institut für Mineralogie, Ruhr-Universität Bochum, Universitätsstrasse 150, D-44780 Bochum, Germany
[3]Département de Physique, B5, Université de Liège, B-4000 Sart-Tilman, Belgium
[4]Department of Chemistry, University of Missouri-Rolla, Missouri 65409-0010, U.S.A.

ABSTRACT

Several compounds of the $Na_2(Mn_{1-x}Fe^{2+}_x)_2Fe^{3+}(PO_4)_3$ solid solution have been hydrothermally synthesized at 400 °C and 1 kbar; pure alluaudite-like compounds have been obtained for $x = 0.00$, 0.25, 0.50, 0.75, and 1.00. Rietveld refinements of the powder X-ray diffraction patterns indicate the presence of Na^+ at the A1 and A2' sites, Mn^{2+} and Fe^{2+} at the M1 site, and Mn^{2+}, Fe^{2+}, and Fe^{3+} at the M2 site. The presence of small amounts of Na^+ at the M1 site and Mn^{2+} at the A1 site indicates a partially disordered distribution of these cations. An excellent linear correlation has been established between the M1-M2 distance and the energy of the infrared band attributed to the M^{2+}-O vibrations. The Mössbauer spectra, measured between 85 and 295 K, were analyzed in terms of a model which includes the next-nearest neighbor interactions at the M2 and M1 crystallographic sites. Fe^{2+} and Fe^{3+} isomer shifts are typical of the alluaudite structure and exhibit the expected second-order Doppler shift. The derived iron vibrating masses and Mössbauer lattice temperatures are within the range of values expected for iron cations in an octahedral environment. The Fe^{2+} and Fe^{3+} quadrupole splittings are typical of the alluaudite structure, and the temperature dependence of the Fe^{2+} quadrupole splitting was fit with the Ingalls model, which yielded a ground state orbital splitting of ca. 460 to 735 cm^{-1} for the Fe^{2+} sites. The isomer shifts and quadrupole splittings of Fe^{2+} at the M1 site are larger than those of Fe^{2+} at M2, indicating that the M1 site is both larger and more distorted than the M2 site.

INTRODUCTION

The crystal structure of natural alluaudite was determined by Moore (1971) in the monoclinic *C*2/*c* space group, and led to the general structural formula $X2X1M1M2_2(PO_4)_3$ with $Z = 4$. However, more recent structural refinements of synthetic phosphates with the alluaudite structure (Yakubovich et al. 1977; Antenucci 1992; Warner et al. 1993; Antenucci et al. 1993, 1995; Lii and Shih 1994; Leroux et al. 1995a, 1995b; Lii and Ye 1997; Korzenski et al. 1998; Hatert et al. 2000, 2002, 2003, 2004; Chouaibi et al. 2001; Guesmi and Driss 2002; Daidouh et al. 2002; Ben Smail and Jouini 2002; Durio et al. 2002; Hidouri et al. 2003) clearly demonstrate the existence of three cationic sites that were not reported by Moore (1971). These sites are located in the channels at crystallographic positions which are different from those of the X1 and X2 sites. Based on detailed structural studies, Hatert et al. (2000) proposed a new general formula, $(A2A2')(A1A1'A1''_2)M1M2_2(PO_4)_3$, for alluaudite-type compounds.

In granitic pegmatites, alluaudite exhibits chemical compositions ranging from $Na_2Mn(Fe^{2+}Fe^{3+})(PO_4)_3$ to $NaMnFe^{3+}_2(PO_4)_3$, with Mn^{2+} or some Ca^{2+} replacing Na^+ at the A1 site, Fe^{2+} replacing Mn^{2+} at the M1 site, and some Mg^{2+} or Mn^{2+} replacing iron at the M2 site, where □ represents a lattice vacancy at the A2' site. The transition between these two end-member compositions corresponds to the substitution mechanism $Na^+ + Fe^{2+} \rightarrow \square + Fe^{3+}$ (Fransolet et al. 1986), and occurs during the oxidation processes affecting the complex phosphate associations within granitic pegmatites, particularly in the beryl-columbite-phosphate subtype of the rare-element pegmatites (Černý 1991). Numerous oxidized Na-Mn-Fe-bearing alluaudite specimens have been synthesized by solid state reactions in air (Hatert et al. 2000, 2004; Hatert 2002a), but only a few compounds containing both Fe^{2+} and Fe^{3+} have been hydrothermally synthesized (Yakubovich et al. 1977; Corbin et al. 1986; Korzenski et al. 1998).

To better understand the crystal chemistry of the weakly oxidized end-members, the $Na_2(Mn_{1-x}Fe^{2+}_x)_2Fe^{3+}(PO_4)_3$ solid solution, with $x = 0.00$, 0.25, 0.50, 0.75, and 1.00, has been synthesized by hydrothermal methods. Rietveld refinements of powder X-ray diffraction patterns, and infrared and Mössbauer spectral studies reveal the structural consequences of the replacement of Mn^{2+} by Fe^{2+} in the octahedral chains of the structure. Mössbauer spectroscopy is an especially valuable tool for this study because it provides accurate information about the cation distributions at the M1 and M2 crystallographic sites (Hermann et al. 2002; Hatert et al. 2003, 2004).

EXPERIMENTAL METHODS

Compounds of the $Na_2(Mn_{1-x}Fe^{2+}_x)_2Fe^{3+}(PO_4)_3$ series, with $x = 0.00$, 0.25, 0.50, 0.75, and 1.00, were hydrothermally synthesized at 400 °C and 1 kbar. Stoichiometric quantities of $NaH_2PO_4 \cdot H_2O$, $FePO_4$, MnO, and FeO were homogenized in a mortar and 100 mg of the mixture was sealed in silver tubes together with 10

* E-mail: fhatert@ulg.ac.be

0003-004X/05/0004–653$05.00/DOI: 10.2138/am.2005.1551

µL of distilled water. The silver tubes, which have an inner diameter of 5 mm, were placed in a conventional hydrothermal apparatus with horizontally arranged Tuttle-type cold-seal vessels (Tuttle 1949) for seven days and then cooled in a stream of cold air. Pressure and temperature errors are estimated to be within ±3% and ±10 °C, respectively.

The powder X-ray diffraction patterns of the compounds were recorded with a Philips PW-3710 diffractometer using 1.9373 Å Fe$K\alpha$ radiation. The unit-cell parameters (Table 1) were calculated with the LCLSQ 8.4 least-squares refinement program (Burnham 1991) from the *d*-spacings calibrated with $Pb(NO_3)_2$ as an internal standard. These unit-cell parameters and the atomic positions reported for $NaMnFe_2(PO_4)_3$ (Hatert et al. 2000) served as starting parameters for the Rietveld refinements which were performed with the DBWS-9807 program of Young et al. (1998). The 2θ range extended from 10 to 100° with a step size of 0.02° and a step time of 15 s. The total number of refined parameters was 55 for $x = 0.00$ and 54 for $x = 0.25$ to 1.00, with 510, 506, 500, 498, and 497 observed reflections for $x = 0.00$, 0.25, 0.50, 0.75, and 1.00, respectively. The final Rietveld plot for $Na_2MnFe^{2+}Fe^{3+}(PO_4)_3$ is shown in Figure 1; fits of equivalent quality were obtained for the other compounds.

The infrared spectra were recorded with a Nicolet NEXUS spectrometer, from 50 scans with a 2 cm^{-1} resolution, over the 400–4000 cm^{-1} region. The samples were prepared by intimately mixing 2 mg of sample with KBr to obtain a 150 mg homogeneous pellet which was subsequently dried for a few hours at 120 °C. To prevent water contamination the measurements were performed under a dry air purge.

The Mössbauer spectra were measured between 85 and 295 K with a constant-acceleration spectrometer which utilized a room-temperature rhodium matrix Co^{57}source and was calibrated at room temperature with α-iron powder. The Mössbauer spectral absorbers contained ca. 24 mg/cm^2 of powder.

The wet chemical analyses were performed using 13 to 20 mg of material. Na, Mn, and Fe were determined with an Analytic Jena Novaa 300 atomic absorption spectrophotometer, whereas P was measured by colorimetry.

Crystal chemistry of $Na_2(Mn_{1-x}Fe_x^{2+})_2Fe^{3+}(PO_4)_3$

X-ray diffraction results

Powder X-ray diffraction patterns of the $Na_2(Mn_{1-x}Fe_x^{2+})_2Fe^{3+}(PO_4)_3$ solid solution indicate that pure alluaudite-like compounds are obtained for all *x* values between 0.00 and 1.00. The reliability factors, positional parameters, site occupancies, and selected interatomic distances and angles obtained from the Rietveld refinements are given in Tables 1, 2, and 3, respectively. The satisfactory values of R_p, R_{wp}, R_{Bragg}, and *S* (Table 1) confirm the reliability of the refinements. A polyhedral representation of the crystal structure of $Na_2MnFe^{2+}Fe^{3+}(PO_4)_3$, projected along the approximate [001] direction, is shown in Figure 2.

It is interesting to note the particularly long P2-O3 distances for $x = 0.00$ and 0.25 (Table 3). Preliminary refinements were performed with a model containing soft restraints for the P-O bonds. The unacceptable increase of the *R* factors with this model

Table 1. Unit-cell parameters and reliability factors for the alluaudite-type compounds, $Na_2(Mn_{1-x}Fe_x^{2+})_2Fe^{3+}(PO_4)_3$ (S.G. *C*2/*c*)

x	0.00	0.25	0.50	0.75	1.00
a (Å)	12.024(4)	11.995(3)	11.944(2)	11.894(4)	11.849(2)
b (Å)	12.629(6)	12.596(4)	12.560(2)	12.536(3)	12.539(1)
c (Å)	6.515(3)	6.495(2)	6.480(1)	6.471(2)	6.486(1)
β (°)	114.58(4)	114.60(3)	114.52(1)	114.49(2)	114.51(1)
V (Å³)	899.6(5)	892.3(3)	884.4(2)	878.1(3)	876.8(1)
R_p (%)*	2.52	2.18	2.14	2.27	2.65
R_{wp} (%)*	3.48	2.90	2.93	3.08	3.83
$R_{exp.}$ (%)*	1.38	1.40	1.46	1.49	1.57
*S**	2.50	2.06	2.00	2.05	2.43
R_{Bragg} (%)*	5.68	4.58	5.61	4.60	5.50

* The forms of the agreement factors are given by Young et al. (1998).

Table 2. Positional (*x*, *y*, *z*), isotropic thermal (*B*) and site occupancy (*N*) parameters for the synthetic alluaudite-type compounds, $Na_2(Mn_{1-x}Fe_x^{2+})_2Fe^{3+}(PO_4)_3$

Site	Atom	Wyckoff	*x*	*y*	*z*	*B* (Å²)	*N*
$Na_2Mn_2Fe^{3+}(PO_4)_3$ ($x = 0.00$)							
A2′	Na	4*e*	0	–0.021(1)	0.25	2.4(7)	0.461(9)
A1	Na	4*b*	0.50	0	0	1.2(5)	0.41(1)
	Mn	4*b*	0.50	0	0	1.2(5)	0.09(1)
M1	Mn	4*e*	0	0.2693(7)	0.25	2.4(4)	0.44(2)
	Na	4*e*	0	0.2693(7)	0.25	2.4(4)	0.06(2)
M2	Mn	8*f*	0.2779(5)	0.6559(4)	0.359(1)	0.5(2)	0.48(2)
	Fe	8*f*	0.2779(5)	0.6559(4)	0.359(1)	0.5(2)	0.50
P1	P	4*e*	0	–0.287(1)	0.25	2.1(3)	0.50
P2	P	8*f*	0.2344(8)	–0.1056(7)	0.134(2)	2.1(3)	1.00
O1	O	8*f*	0.463(1)	0.710(1)	0.553(3)	0.9(3)	1.00
O2	O	8*f*	0.089(1)	0.6318(8)	0.247(2)	0.9(3)	1.00
O3	O	8*f*	0.334(1)	0.671(1)	0.114(2)	0.9(3)	1.00
O4	O	8*f*	0.137(1)	0.398(1)	0.340(2)	0.9(3)	1.00
O5	O	8*f*	0.232(1)	0.823(1)	0.319(3)	0.9(3)	1.00
O6	O	8*f*	0.327(1)	0.503(1)	0.393(2)	0.9(3)	1.00
$Na_2Mn_{1.5}Fe_{0.5}^{2+}Fe^{3+}(PO_4)_3$ ($x = 0.25$)							
A2′	Na	4*e*	0	–0.013(1)	0.25	1.0	0.339(4)
A1	Na	4*b*	0.50	0	0	1.8(3)	0.411(7)
	Mn	4*b*	0.50	0	0	1.8(3)	0.089(7)
M1	Mn	4*e*	0	0.2676(4)	0.25	1.0(3)	0.47(1)
	Na	4*e*	0	0.2676(4)	0.25	1.0(3)	0.03(1)
M2	Mn	8*f*	0.2779(4)	0.6557(2)	0.3623(7)	0.6(1)	0.21(4)
	Fe	8*f*	0.2779(4)	0.6557(2)	0.3623(7)	0.6(1)	0.75
P1	P	4*e*	0	–0.2822(6)	0.25	0.9(2)	0.50
P2	P	8*f*	0.2343(5)	–0.1074(4)	0.130(1)	0.9(2)	1.00
O1	O	8*f*	0.4593(8)	0.7109(9)	0.535(2)	0.5(2)	1.00
O2	O	8*f*	0.1043(9)	0.6383(6)	0.249(1)	0.5(2)	1.00
O3	O	8*f*	0.3360(8)	0.6702(7)	0.115(2)	0.5(2)	1.00
O4	O	8*f*	0.1293(8)	0.3980(7)	0.332(1)	0.5(2)	1.00
O5	O	8*f*	0.2279(7)	0.8257(8)	0.318(2)	0.5(2)	1.00
O6	O	8*f*	0.3262(7)	0.5017(9)	0.388(1)	0.5(2)	1.00
$Na_2MnFe^{2+}Fe^{3+}(PO_4)_3$ ($x = 0.50$)							
A2′	Na	4*e*	0	–0.0113(7)	0.25	1.2(4)	0.380(5)
A1	Na	4*b*	0.50	0	0	1.6(3)	0.489(5)
M1	Mn	4*e*	0	0.2690(3)	0.25	1.0(2)	0.520(4)
M2	Fe	8*f*	0.2795(3)	0.6573(2)	0.3641(5)	1.0(1)	0.982(7)
P1	P	4*e*	0	–0.2846(5)	0.25	1.0	0.50
P2	P	8*f*	0.2370(4)	–0.1106(3)	0.1238(9)	1.0	1.00
O1	O	8*f*	0.4584(7)	0.7139(6)	0.538(1)	1.1(1)	1.00
O2	O	8*f*	0.1027(8)	0.6433(5)	0.239(1)	1.1(1)	1.00
O3	O	8*f*	0.3365(7)	0.6703(5)	0.110(1)	1.1(1)	1.00
O4	O	8*f*	0.1270(7)	0.3992(5)	0.328(1)	1.1(1)	1.00
O5	O	8*f*	0.2283(6)	0.8256(6)	0.326(1)	1.1(1)	1.00
O6	O	8*f*	0.3235(6)	0.4947(7)	0.384(1)	1.1(1)	1.00
$Na_2Mn_{0.5}Fe_{1.5}^{2+}Fe^{3+}(PO_4)_3$ ($x = 0.75$)							
A2′	Na	4*e*	0	–0.0110(7)	0.25	1.9(4)	0.376(5)
A1	Na	4*b*	0.50	0	0	2.2(3)	0.510(5)
M1	Mn	4*e*	0	0.2687(3)	0.25	0.3(2)	0.221(3)
	Fe	4*e*	0	0.2687(3)	0.25	0.3(2)	0.25
M2	Fe	8*f*	0.2803(3)	0.6576(2)	0.3655(4)	0.89(9)	0.990(6)
P1	P	4*e*	0	–0.2845(4)	0.25	1.0	0.50
P2	P	8*f*	0.2375(4)	–0.1096(3)	0.1243(8)	1.0	1.00
O1	O	8*f*	0.4575(6)	0.7129(6)	0.536(1)	1.2(1)	1.00
O2	O	8*f*	0.1034(7)	0.6419(4)	0.242(1)	1.2(1)	1.00
O3	O	8*f*	0.3347(6)	0.6671(5)	0.109(1)	1.2(1)	1.00
O4	O	8*f*	0.1278(6)	0.4012(5)	0.329(1)	1.2(1)	1.00
O5	O	8*f*	0.2270(6)	0.8261(6)	0.323(1)	1.2(1)	1.00
O6	O	8*f*	0.3215(5)	0.4996(7)	0.3829(9)	1.2(1)	1.00
$Na_2Fe_2^{2+}Fe^{3+}(PO_4)_3$ ($x = 1.00$)							
A2′	Na	4*e*	0	–0.0117(7)	0.25	1.0	0.377(2)
A1	Na	4*b*	0.50	0	0	0.4(3)	0.474(5)
M1	Fe	4*e*	0	0.2688(2)	0.25	1.3(2)	0.504(4)
M2	Fe	8*f*	0.2819(3)	0.6580(2)	0.3674(5)	1.38(9)	1.051(8)
P1	P	4*e*	0	–0.2866(4)	0.25	0.4(1)	0.50
P2	P	8*f*	0.2330(4)	–0.1097(3)	0.1230(8)	0.4(1)	1.00
O1	O	8*f*	0.4580(7)	0.7196(5)	0.541(1)	0.5(1)	1.00
O2	O	8*f*	0.0989(7)	0.6354(4)	0.239(1)	0.5(1)	1.00
O3	O	8*f*	0.3327(6)	0.6668(5)	0.109(1)	0.5(1)	1.00
O4	O	8*f*	0.1300(7)	0.3976(4)	0.329(1)	0.5(1)	1.00
O5	O	8*f*	0.2230(7)	0.8275(5)	0.321(1)	0.5(1)	1.00
O6	O	8*f*	0.3252(5)	0.5020(6)	0.389(1)	0.5(1)	1.00

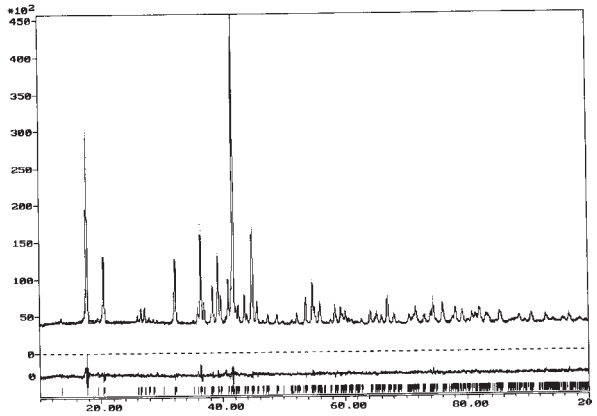

FIGURE 1. The observed (dots), calculated (solid line), and difference powder X-ray diffraction patterns of $Na_2MnFe^{2+}Fe^{3+}(PO_4)_3$ obtained from a Rietveld refinement. The vertical markers indicate the calculated positions of the Fe$K\alpha_1$ and Fe$K\alpha_2$ Bragg reflections.

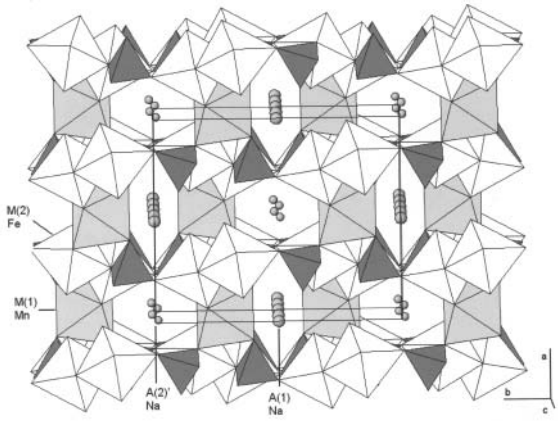

FIGURE 2. The projection of the crystal structure of $Na_2MnFe^{2+}Fe^{3+}(PO_4)_3$. The PO_4 tetrahedra are densely shaded. The shaded M1 octahedra are occupied by Mn^{2+}, and the unshaded M2 octahedra are occupied by iron. The circles indicate Na^+ at the A1 and A2' crystallographic sites.

confirms the distortion of the $P2O_4$ tetrahedron.

The crystallographic sites of the alluaudite-like compounds (Table 2) are labeled according to the nomenclature recently proposed by Hatert et al. (2000). The morphologies of the coordination polyhedra of M1 and M2 are those of distorted octahedra, whereas the morphologies of A1 and A2' are those of a distorted cube and of a gabled disphenoid, respectively. These morphologies are similar to those previously described for the $(Na_{1-x}Li_x)MnFe_2(PO_4)_3$ compounds (Hatert et al. 2000).

Because iron and manganese cannot be distinguished from Rietveld refinements of X-ray diffraction data the Fe-content of the M2 site was fixed to its theoretical value for $x = 0.00$ and 0.25, whereas the occupancy factors (Table 2) indicate that this site is filled with Fe for $x = 0.50$ to 1.00. Preliminary refinements were performed by assuming that Mn^{2+} is at the M1 site and Na^+ is at the A1 site. For $x = 0.00$ and 0.25 these refinements showed a rather low electronic density at the M1 site, whereas the electronic density at the A1 site was particularly high when compared with the theoretical values. This behavior is likely related to the presence of small amounts of Na^+ at the M1 site, and of Mn^{2+} or Fe^{2+} at the A1 site. Because the effective ionic radius of Na^+ is closer to the effective ionic radius of Mn^{2+} than to that of Fe^{2+} (Shannon 1976) we chose a simple model with Na^+ and Mn^{2+} at A1 and M1. Consequently, the occupancy factors for the A1 and M1 sites (Table 2) are calculated assuming a full occupancy by Na^+ and Mn^{2+}.

This partially disordered distribution of Na^+ and Mn^{2+} between the A1 and M1 sites (Table 2) was previously observed by Hatert (2002a) in the alluaudite-like $Na_2Mn_2Fe^{3+}(PO_4)_3$ and $Na_2Mn_2Ga(PO_4)_3$ compounds, synthesized by solid state reactions. The progressive replacement of Mn^{2+} by Fe^{2+} in the alluaudite structure induces a significant decrease in the unit-cell parameters (Table 1) and mean M1-O distances (Table 3), which prevent the incorporation of Na^+ at the M1 site for $x =$ 0.50 to 1.00.

The occupancy factors given in Table 2 also indicate that the A2' site is not completely filled with Na^+. The occurrence of vacancies in this crystallographic site cannot be ruled out, because natural oxidized alluaudite specimens exhibit compositions close to $\square NaMnFe^{3+}_2(PO_4)_3$ or $\square NaFe^{2+}Fe^{3+}_2(PO_4)_3$ (Fransolet et al. 1985, 1986). Small changes in the oxygen fugacity during synthesis can therefore lead to oxidation of Fe^{2+} to Fe^{3+}, which is coupled with replacement of Na^+ by vacancies through the $Na^+ + Fe^{2+} \rightarrow \square + Fe^{3+}$ substitution mechanism. The Mössbauer spectral study helped to determine the oxidation state of iron in the alluaudite-type compounds considered in this paper.

Variation of the unit-cell parameters

The unit-cell parameters of the $Na_2(Mn_{1-x}Fe^{2+}_x)_2Fe^{3+}(PO_4)_3$ alluaudite-like compounds given in Table 1 show an essentially linear decrease with increasing x, a decrease which results from the replacement of Mn^{2+} by Fe^{2+} at the M1 and M2 crystallographic sites. This decrease (Fig. 3) correlates with the variation of the bond distances induced by the incorporation of Fe^{2+} into the alluaudite structure. The differences between the bond distances in $Na_2Mn_2Fe^{3+}(PO_4)_3$ and $Na_2Fe^{2+}_2Fe^{3+}(PO_4)_3$, see Table 3, clearly indicate that significant variations in the bond distances occur for the M1 and M2 crystallographic sites.

As has been shown by Hatert (2002a) and Hatert et al. (2003), variations in the M2-O bond distances significantly affect the b unit-cell parameter, whereas variations in the M1-O distances affect the a parameter. For $x = 0.00$ to 0.50, the incorporation of Fe^{2+} at the M2 site (Table 2) provokes a significant decrease in the b parameter, whereas the decrease in a is smaller (Fig. 3). For $x = 0.50$ to 1.00, Fe^{2+} is introduced to the M1 site (Table 2), thus inducing a more significant decrease in a as compared to b (Fig. 3).

As is shown in Figure 4, the significant decrease in the β angle correlates with the M1-M2 distances given in Table 3. Similar correlations have been previously established by Hatert (2002a) and Hatert et al. (2003) for the $Na_{1.5}(Mn_{1-x}Cd_x)_{1.5}Fe^{3+}_{1.5}(PO_4)_3$, $Na_{1.5}(Mn_{1-x}Zn_x)_{1.5}Fe^{3+}_{1.5}(PO_4)_3$, and $NaMn(Fe^{3+}_{1-x}In_x)_2(PO_4)_3$ alluaudite-type solid solutions. However, the correlations previously observed were better than those presented in Figure 4, probably

TABLE 3. Selected interatomic distances (Å) and angles (°) for the synthetic alluaudite-type compounds, $Na_2(Mn_{1-x}Fe^{2+}_x)_2Fe^{3+}(PO_4)_3$

x	0.00	0.25	0.50	0.75	1.00	Difference
A2′-O6 ×2	2.40(1)	2.411(6)	2.442(6)	2.447(5)	2.401(6)	+0.00
A2′-O6 ×2	2.627(8)	2.596(6)	2.593(5)	2.604(4)	2.585(4)	–0.04
A2′-O1 ×2	2.66(2)	2.80(2)	2.84(1)	2.83(1)	2.89(1)	0.23
A2′-O3 ×2	3.03(2)	2.92(1)	2.893(9)	2.863(9)	2.876(9)	–0.15
Mean	2.68	2.68	2.69	2.69	2.69	0.01
A1-O2 ×2	2.25(1)	2.352(7)	2.359(6)	2.352(5)	2.270(5)	0.02
A1-O4 ×2	2.50(1)	2.433(7)	2.397(6)	2.386(6)	2.418(6)	–0.08
A1-O4 ×2	2.625(9)	2.580(7)	2.559(6)	2.542(5)	2.582(6)	–0.04
A1-O2 ×2	2.85(1)	2.993(7)	3.054(6)	3.028(6)	2.961(6)	0.11
Mean	2.56	2.59	2.59	2.58	2.56	0.00
M1-O1 ×2	2.32(1)	2.22(1)	2.231(6)	2.224(6)	2.229(6)	–0.09
M1-O4 ×2	2.21(1)	2.168(9)	2.143(7)	2.165(6)	2.142(6)	–0.07
M1-O3 ×2	2.20(1)	2.170(8)	2.169(6)	2.198(6)	2.213(6)	0.01
Mean	2.24	2.19	2.18	2.20	2.19	–0.05
M2-O3	1.98(1)	2.01(1)	2.033(6)	2.019(6)	2.005(6)	0.03
M2-O6	2.00(1)	2.01(1)	2.099(9)	2.032(9)	2.012(8)	0.01
M2-O2	2.099(8)	1.910(8)	1.930(7)	1.926(6)	1.994(6)	–0.11
M2-O1	2.16(1)	2.108(8)	2.084(7)	2.052(6)	2.066(6)	–0.09
M2-O5	2.17(2)	2.12(1)	2.060(6)	2.063(6)	2.054(7)	–0.12
M2-O5	2.17(1)	2.21(1)	2.186(8)	2.190(8)	2.218(7)	0.05
Mean	2.10	2.06	2.07	2.05	2.06	–0.04
M1-M2	3.356(5)	3.352(4)	3.327(3)	3.308(3)	3.290(3)	–0.07
P1-O2 ×2	1.49(1)	1.605(9)	1.550(8)	1.555(6)	1.551(6)	0.06
P1-O1 ×2	1.52(2)	1.56(1)	1.535(7)	1.549(7)	1.494(7)	–0.03
Mean	1.51	1.58	1.54	1.55	1.52	0.01
P2-O4	1.485(8)	1.551(8)	1.527(6)	1.508(5)	1.524(6)	0.04
P2-O5	1.52(2)	1.51(1)	1.576(8)	1.566(7)	1.552(7)	0.03
P2-O6	1.53(1)	1.54(1)	1.498(9)	1.530(9)	1.549(8)	0.02
P2-O3	1.69(2)	1.66(1)	1.589(8)	1.569(7)	1.553(8)	–0.14
Mean	1.56	1.56	1.55	1.54	1.54	–0.02
O2-P1-O2	92.9(9)	102.8(6)	108.5(5)	107.2(4)	101.8(4)	
O1-P1-O1	101(1)	109.6(8)	109.3(5)	109.2(5)	111.6(5)	
O2-P1-O1 ×2	112.9(5)	108.1(4)	105.4(3)	106.5(3)	106.7(3)	
O2-P1-O1 ×2	119.5(6)	114.2(4)	114.3(3)	113.8(3)	115.0(3)	
Mean	109.8	109.5	109.5	109.5	109.5	
O4-P2-O3	101.2(7)	104.8(4)	110.7(4)	110.3(4)	106.8(4)	
O6-P2-O3	107.9(8)	108.6(5)	108.5(4)	108.7(4)	109.5(4)	
O6-P2-O5	117.1(8)	112.3(5)	106.2(4)	107.1(4)	108.4(4)	
O5-P2-O3	107.9(9)	109.4(6)	110.6(4)	110.8(4)	112.8(4)	
O6-P2-O4	114.5(8)	114.0(5)	113.2(4)	111.2(4)	111.7(3)	
O4-P2-O5	106.9(8)	107.5(5)	107.6(4)	108.7(4)	107.6(4)	
Mean	109.3	109.4	109.5	109.5	109.5	

because the replacement of Mn^{2+} by Fe^{2+} induces a smaller change in the M1-M2 distance (Table 3) as compared to the significant variations observed by Hatert (2002a) and Hatert et al. (2003). This is due to the similar effective ionic radii of 0.830 Å for Mn^{2+} and 0.780 Å for Fe^{2+} (Shannon 1976).

Infrared spectroscopy

The infrared spectra of $Na_2(Mn_{1-x}Fe^{2+}_x)_2Fe^{3+}(PO_4)_3$, shown in Figure 5, are typical of an orthophosphate structure (Rulmont et al. 1991). Because the infrared spectra of alluaudite samples exhibit a complexity which is related both to the low symmetry and to the large unit-cell of the alluaudite structure (Antenucci et al. 1993), it is difficult to assign all the individual absorption bands. Nevertheless, the spectra of $Na_2(Mn_{1-x}Fe^{2+}_x)_2Fe^{3+}(PO_4)_3$ can be assigned through comparison with the similar spectra of $NaCdIn_2(PO_4)_3$ and $NaMn(Fe_{1-x}In_x)_2(PO_4)_3$ published by Antenucci et al. (1993) and Hatert et al. (2003). According to these

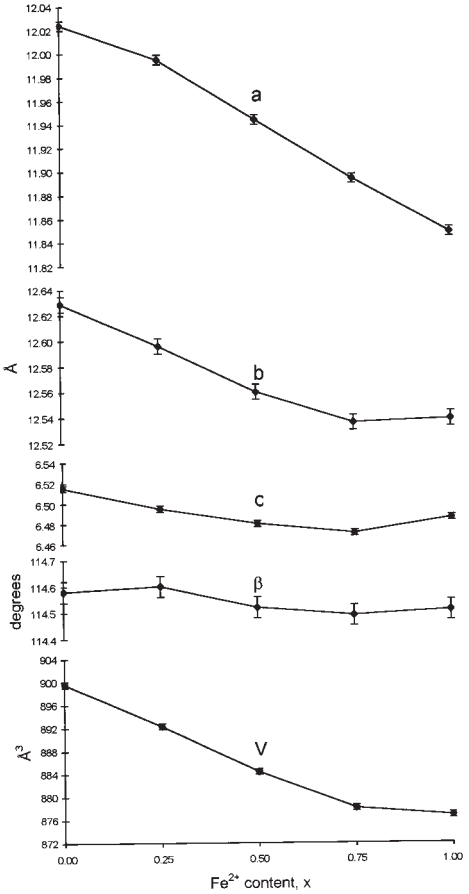

FIGURE 3. The compositional dependence of the unit-cell parameters of $Na_2Mn_{1-x}Fe^{2+}_x)_2Fe^{3+}(PO_4)_3$. The error bars are smaller than the data points.

authors, the stretching vibrational modes of the PO_4 tetrahedra occur in the 1200–850 cm^{-1} region, while the PO_4 bending vibrational modes occur between ca. 400 and 650 cm^{-1}. Starting from these hypotheses, a more detailed assignment of the absorption bands is presented in Table 4.

According to the fundamental vibrational frequencies of the PO_4 tetrahedron given by Farmer (1974), the absorption bands between 930 and 1094 cm^{-1} can be assigned to ν_3, the antisymmetric stretching modes of the PO_4 anions, and the bands between 545 and 584 cm^{-1} can be assigned to ν_4, their bending mode. The bands at 520 and 595 cm^{-1} in the spectrum of $Na_2Fe^{2+}_2Fe^{3+}(PO_4)_3$ are more difficult to assign, whereas the weak band at 909 cm^{-1} probably corresponds to ν_1, the symmetric stretching mode of the distorted PO_4 tetrahedron.

When the Fe^{2+}-content of the $Na_2(Mn_{1-x}Fe^{2+}_x)_2Fe^{3+}(PO_4)_3$ solid solution increases, the infrared spectra show an important displacement of an absorption band found at 433 cm^{-1} in the spectrum of $Na_2Fe^{2+}_2Fe^{3+}(PO_4)_3$ (Table 4). This band can be assigned to the Mn^{2+}-O and Fe^{2+}-O vibrations, an assignment which is confirmed by the excellent correlation between the M1-M2 bond distance and the energy of the absorption band (Fig. 6).

White and Keramidas (1972) studied the infrared spectra of several oxides and established a linear correlation between the

highest frequency band in the spectra and the M^{3+}-O bond distance. According to this correlation, the highest frequency band at 653 cm^{-1} for the Fe^{3+}-O vibrational mode in the spectrum of $Na_2Fe_2^{2+}Fe^{3+}(PO_4)_3$ corresponds to a Fe^{3+}-O distance of 2.08 Å, a value which is close to the mean M2-O bond length of 2.06 Å (Table 3).

Fe^{57} Mössbauer spectroscopy

The 85 K Mössbauer spectra of $Na_2(Mn_{1-x}Fe_x^{2+})_2Fe^{3+}(PO_4)_3$, with x = 0.00, 0.25, 0.50, 0.75, and 1.00, are shown in Figure 7 and the spectra of $Na_2Mn_{0.5}Fe_{1.5}^{2+}Fe^{3+}(PO_4)_3$, obtained at four different temperatures, are shown in Figure 8. The general appearance of these spectra indicate that they should be fit with at least two doublets, one assigned to Fe^{2+} with a large isomer shift and quadrupole splitting, and a second assigned to Fe^{3+} and having a small isomer shift and quadrupole splitting. However, both the poor fits and the broad linewidths obtained from such preliminary fits reveal that a reasonable spectral fit will require at least two Fe^{2+} doublets and two Fe^{3+} doublets.

Three different models for the Mössbauer spectral analysis have been developed, based on the previous investigations by Hermann et al. (2002) and Hatert et al. (2003, 2004). The first model has been used for x = 0.00 and 0.25, and considers a random distribution of Fe^{2+}, Fe^{3+}, and Mn^{2+} at the M2 site, while the M1 site is filled with Mn^{2+}. In this model, six different next-nearest neighbor iron environments are possible (Fig. 9). Thus, if f represents the Fe^{2+} fraction of the total iron content of the M2 site, the probabilities given in Figure 9 for the six different iron environments are obtained. Under these assumptions, the Mössbauer spectra should exhibit three Fe^{2+} and three Fe^{3+} quadrupole doublets. A fit with these assumptions would require 21 adjustable parameters, but preliminary fits indicated that the isomer shifts and linewidths of the three Fe^{2+} and three Fe^{3+} doublets were identical within experimental error. Thus, the final fits involved the adjustment of only 13 parameters, one Fe^{2+} fraction, f, two isomer shifts, δ, six quadrupole splittings, ΔE_Q, and two linewidths, Γ, as well as the total spectral area and spectral baseline. For x = 0.00, however, the very low amount of Fe^{2+}, ca. 8%, makes it impossible to obtain a satisfactory fit. For this reason, the values of ΔE_Q for Fe^{2+} were constrained to the values obtained for x = 0.25.

The second model, applied for x = 0.50, is similar to that developed by Hermann et al. (2002), in which a random distribution of Fe^{2+} and Fe^{3+} occurs at M2, whereas M1 is filled with Mn^{2+} (Fig. 9). The Mössbauer spectra should therefore show two Fe^{2+} and two Fe^{3+} doublets. The fits involved the adjustment of 11 parameters, one Fe^{2+} fraction, f, two isomer shifts, δ, four quadrupole splittings, ΔE_Q, and two linewidths, Γ, as well as the total spectral area and spectral baseline.

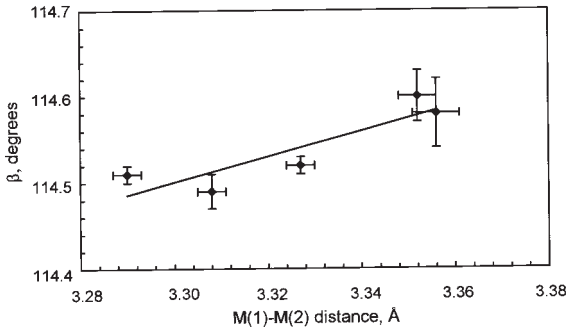

FIGURE 4. Correlation between the β angle and the M1-M2 distance in the $Na_2(Mn_{1-x}Fe_x^{2+})_2Fe^{3+}(PO_4)_3$ alluaudite-type compounds.

TABLE 4. Assignments of the infrared frequencies (cm^{-1}) for the alluaudite-type compounds, $Na_2(Mn_{1-x}Fe_x^{2+})_2Fe^{3+}(PO_4)_3$

0.00	0.25	0.50	0.75	1.00	Difference	Assignment
1082	1089	1097	1097	1094	12	ν_3 PO_4
		1044	1044		–	ν_3 PO_4
990	992	993	1004	1001	11	ν_3 PO_4
930	938	941	942	936	6	ν_3 PO_4
		924	919	909	–	ν_1 PO_4 ?
				653	–	Fe^{3+}-O
634	634	634		638	4	Fe^{3+}-O
602	602	596	596	595	–7	Fe^{3+}-O or ν_4 PO_4 ?
583	584	581	581	580	–3	ν_4 PO_4
	575				–	ν_4 PO_4
545	545	545	546	545	0	ν_4 PO_4
516	518	520	517	520	4	$(Fe,Mn)^{2+}$-O or ν_4 PO_4 ?
466	467	465	464	463	–3	Fe^{3+}-O or PO_4 bending ?
415	417	422	427	433	18	$(Fe,Mn)^{2+}$-O

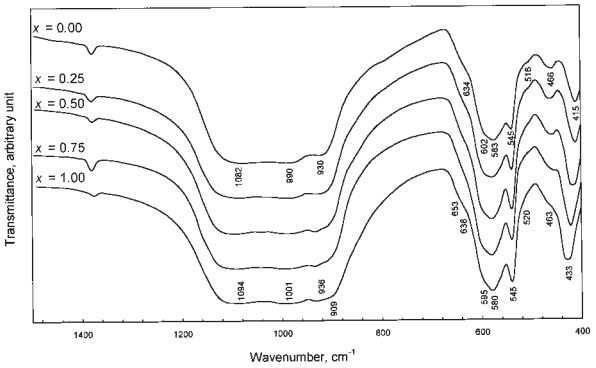

FIGURE 5. The infrared spectra of the $Na_2(Mn_{1-x}Fe_x^{2+})_2Fe^{3+}(PO_4)_3$ alluaudite-type compounds.

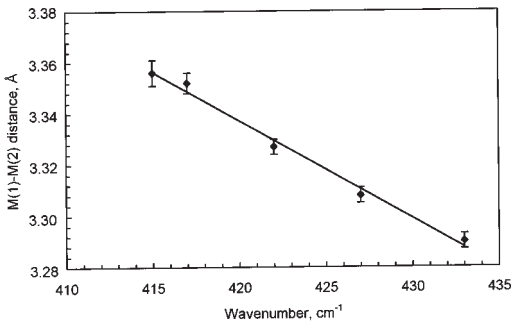

FIGURE 6. Correlation between the M1-M2 distance and the energy of the infrared absorption band assigned to the Fe^{2+}-O and Mn^{2+}-O vibrations in the $Na_2(Mn_{1-x}Fe_x^{2+})_2Fe^{3+}(PO_4)_3$ alluaudite-type compounds.

The last model was used to fit the spectra of the compounds with $x = 0.75$ and 1.00. In these samples, the occupancy of M2 is the same as that observed for $x = 0.50$, but a disordered distribution of Mn^{2+} and Fe^{2+} occurs at M1. We consider that Fe^{3+} does not occupy the M1 site, because the effective ionic radius of this cation, 0.645 Å, is very small, compared to the effective ionic radii of 0.780 and 0.830 Å for Fe^{2+} and Mn^{2+}, respectively (Shannon 1976). Consequently, the interactions between Fe^{2+} localized at M1 and the cations occurring at the adjoining M2 site must be taken into account (Fig. 9). According to this model, the Mössbauer spectra should exhibit three M1 Fe^{2+} doublets, two M2 Fe^{2+} doublets, and two M2 Fe^{3+} doublets. However, preliminary fits with this model were unsatisfactory, probably because the number of parameters was too high. For this reason, the less probable M1 Fe^{2+} doublet was neglected (Fig. 9), and the final fits involved the adjustment of 15 parameters, one Fe^{2+} fraction, f, three isomer shifts, δ, six quadrupole splittings, ΔE_Q, and three linewidths, Γ, as well as the total spectral area and spectral baseline. The resulting fits are excellent, as is shown in Figures 7 and 8; the best-fit hyperfine parameters are given in Table 5.

In agreement with the second order Doppler shift (Herber 1984), both the Fe^{2+} and Fe^{3+} isomer shifts decrease with increasing temperature, as is shown in Figure 10 for $Na_2Mn_{0.5}Fe^{2+}_{1.5}Fe^{3+}(PO_4)_3$. A comparable linear behavior was observed for all the other compounds under study herein and the zero temperature intercepts, $\delta(0)$, and the slopes, $d\delta/dT$, are given in Table 6. The temperature dependence of the logarithm of the absorption area was fit with the Debye model (Herber 1984) in which the mass of the iron nuclide was fixed at 57 g/mol. The Debye or Mössbauer lattice temperatures obtained from these fits for the $Na_2(Mn_{1-x}Fe_x^{2+})_2Fe^{3+}(PO_4)_3$ alluaudite-type compounds are given in Table 6. Debye temperatures between 320 and 430 K are typical for iron in the octahedral sites of the spinel structure (Vandenberghe and De Grave 1989).

As expected, the high-spin Fe^{3+} quadrupole splittings, $\Delta E_{Q,3\text{-}3}$, $\Delta E_{Q,3\text{-}2}$, and $\Delta E_{Q,3\text{-}Mn}$ are independent of temperature within experimental error (Fig. 11). In contrast, but as expected, the high-spin Fe^{2+} quadrupole splittings, $\Delta E_{Q,2\text{-}2}$, $\Delta E_{Q,2\text{-}3}$, and $\Delta E_{Q,2\text{-}Mn}$, increase substantially with cooling (Fig. 11). The temperature dependence of the Fe^{2+} quadrupole splitting, ΔE_Q, in a distorted environment may be calculated (Ingalls 1964) from the expression,

$$\Delta E_Q = \Delta E_Q(0) \times \{1 - \exp(-\Delta/kT)\}/\{1 + 2\exp(-\Delta/kT)\},$$

where $\Delta E_Q(0)$ is the quadrupole splitting at 0 K and Δ is the

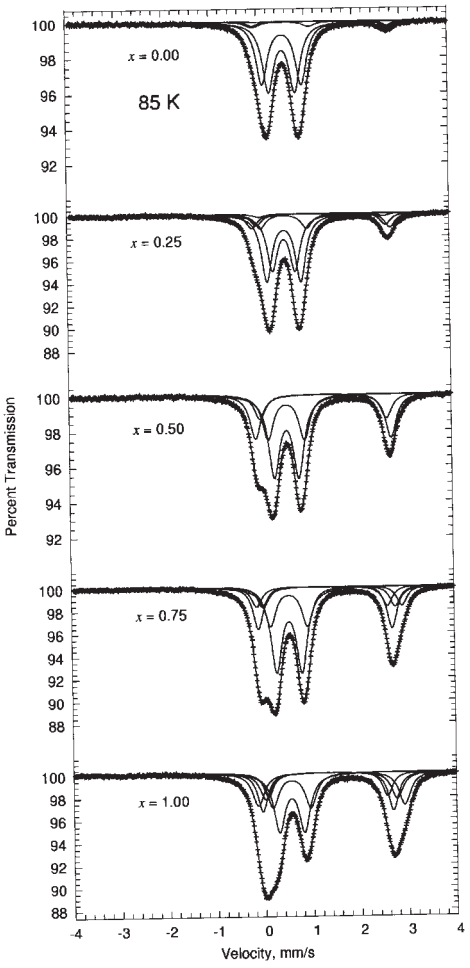

FIGURE 7. The Mössbauer spectra of $Na_2(Mn_{1-x}Fe_x^{2+})_2Fe^{3+}(PO_4)_3$ obtained at 85 K.

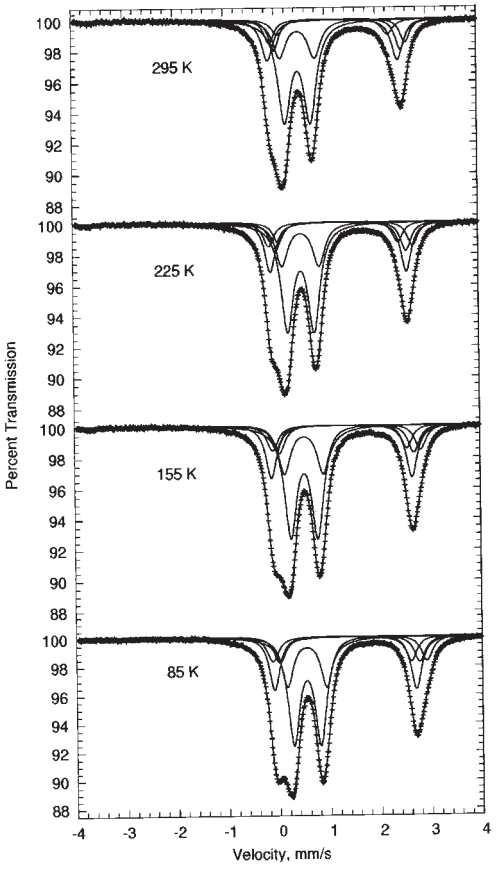

FIGURE 8. The Mössbauer spectra of $Na_2Mn_{0.5}Fe^{2+}_{1.5}Fe^{3+}(PO_4)_3$ obtained at the indicated temperatures.

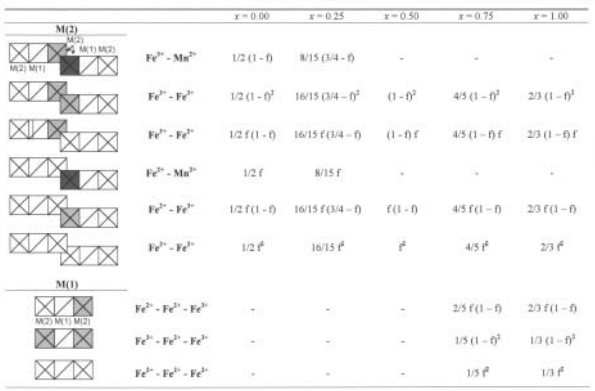

FIGURE 9. The nine different configurations of next-nearest neighbor M sites occupied by Fe^{3+} (shaded), Fe^{2+} (white), and Mn (densely shaded) in the $Na_2(Mn_{1-x}Fe^{2+}_x)_2Fe^{3+}(PO_4)_3$ alluaudite-type compounds. The calculated probabilities are shown for $x = 0.00$ to 1.00.

low-symmetry crystal field splitting of the octahedral Fe^{2+} orbital triplet ground state. It should be noted that an incorrect equation was used by Hermann et al. (2002) and Hatert et al. (2003) to fit the temperature dependence of the Fe^{2+} quadrupole splittings. The solid lines shown in Figure 11 correspond to the best fits of the quadrupole splittings with the Ingalls model and the parameters are given in Table 6. A splitting of 500 to 700 cm^{-1} is rather normal for a distorted octahedral environment (Hartmann-Boutron and Imbert 1968). These values are similar to those given by Hatert et al. (2004), with $\Delta_{2\text{-}3}$ significantly larger than $\Delta_{2\text{-}2}$ (Table 6). The failure of the Ingalls model to more adequately fit the Fe^{2+}-Fe^{3+} quadrupole splittings (Fig. 11) is an indication that the low-symmetry components of the octahedral crystal field are changing with temperature, changes which are not considered by the Ingalls model. Indeed, such changes are expected in alluaudite-like compounds which have a non-compact crystal structure.

DISCUSSION

This paper reports both the first hydrothermal synthesis of a complete solid solution of Na-Mn-Fe-bearing alluaudite specimens and their crystal-chemical characterization. It is important to note that the hydrothermal synthesis of alluaudite specimens with chemical compositions close to those of natural primary alluaudite specimens (Fransolet et al. 1985, 1986) constitutes a very promising result, because preliminary data concerning the stability of alluaudite have been obtained with this technique (Hatert 2002a, 2002b; Hatert and Fransolet 2002).

Rietveld refinements of the powder X-ray diffraction patterns have shown a partially disordered distribution between Na^+ and Mn^{2+} at the A1 and M1 crystallographic sites. The presence of vacancies at the A2' site has also been observed herein. According to the oxidation mechanism corroborated by Fransolet et al. (1985, 1986), $Na^+ + Fe^{2+} \rightarrow \square + Fe^{3+}$, alluaudite samples containing vacancies are also enriched in Fe^{3+}, compared to the nominal compositions. The Rietveld refinements show the presence of 0.24 to 0.32 vacancies for $x = 0.25$ to 1.00, whereas the number of vacancies per formula unit is only 0.08 for $x = 0.00$. Beginning with the fraction of Fe^{2+} obtained from the 85

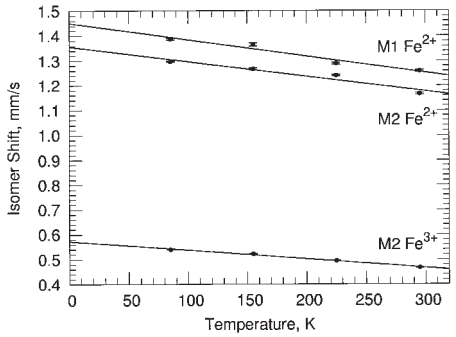

FIGURE 10. The temperature dependence of the isomer shifts of $Na_2Mn_{0.5}Fe^{2+}_{1.5}Fe^{3+}(PO_4)_3$.

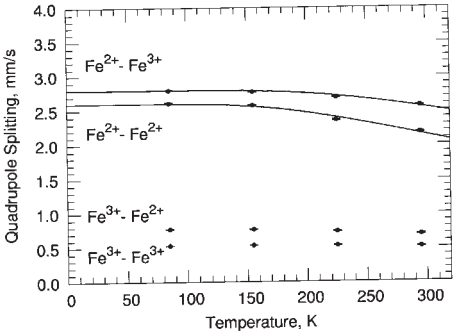

FIGURE 11. The temperature dependence of the M2 quadrupole splittings of $Na_2Mn_{0.5}Fe^{2+}_{1.5}Fe^{3+}(PO_4)_3$.

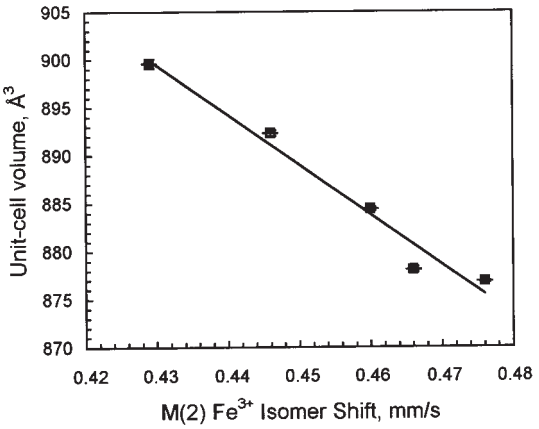

FIGURE 12. Correlation between the M2 Fe^{3+} isomer shift and the unit-cell volume in the $Na_2(Mn_{1-x}Fe^{2+}_x)_2Fe^{3+}(PO_4)_3$ alluaudite-type compounds.

K Mössbauer spectrum, we can calculate the excess amount of Fe^{3+}, an amount which corresponds to the number of vacancies per formula unit. For $x = 0.25$ to 1.00 the calculated number of vacancies is between 0.23 and 0.36, whereas an excess of Fe^{2+} in $Na_2Mn_2Fe^{3+}(PO_4)_3$ indicates that the A2' site is completely filled with Na^+. These calculated values are in excellent agreement with the number of vacancies obtained from the Rietveld refinements of the powder X-ray diffraction patterns.

TABLE 5. Mössbauer spectral parameters for $Na_2(Mn_{1-x}Fe^{2+}_x)_2Fe^{3+}(PO_4)_3$

		A		M2 Fe^{3+} (mm/s)					M2 Fe^{2+} (mm/s)				
x	T (K)	[(%ε)(mm/s)]/(mg/cm^2)	f (%)	δ*	$\Delta E_{Q,3\text{-}3}$	$\Delta E_{Q,3\text{-}2}$	$\Delta E_{Q,3\text{-}Mn}$	Γ	δ*	$\Delta E_{Q,2\text{-}3}$	$\Delta E_{Q,2\text{-}2}$	$\Delta E_{Q,2\text{-}Mn}$	Γ
0.00	85	−7.49(2)	7.9(2)	0.531(1)	0.823(2)	1.14(3)	0.549(2)	0.288(2)	1.322(5)	2.892†	2.59†	2.75(2)	0.28(1)
	155	−7.16(2)	7.8(3)	0.508(1)	0.814(2)	1.12(3)	0.549(2)	0.292(2)	1.285(5)	2.838†	2.6†	2.67(2)	0.27(1)
	225	−6.74(2)	6.7(3)	0.470(1)	0.802(3)	1.07(4)	0.548(2)	0.302(3)	1.233(5)	2.75†	2.47†	2.62(2)	0.26(1)
	295	−6.55(2)	7.1(3)	0.429(1)	0.796(3)	1.06(4)	0.539(3)	0.304(3)	1.170(6)	2.652†	1.75†	2.51(2)	0.28(1)
0.25	85	−12.22(3)	13.4(1)	0.533(1)	0.709(1)	0.968(7)	0.475(2)	0.267(2)	1.316(1)	2.892(7)	2.59(4)	2.69(1)	0.263(7)
	155	−11.78(3)	13.3(1)	0.514(1)	0.705(1)	0.963(7)	0.469(2)	0.268(2)	1.291(1)	2.838(9)	2.6(1)	2.66(2)	0.271(8)
	225	−11.33(3)	12.7(2)	0.486(1)	0.698(1)	0.950(8)	0.471(2)	0.276(2)	1.255(1)	2.75(1)	2.47(4)	2.60(1)	0.268(9)
	295	−10.69(3)	12.5(1)	0.446(1)	0.689(1)	0.925(9)	0.467(2)	0.272(2)	1.204(1)	2.652(8)	1.75(3)	2.48(1)	0.256(8)
0.50	85	−9.64(3)	35.8(2)	0.538(1)	0.514(2)	0.758(4)	–	0.281(2)	1.313(1)	2.835(3)	2.634(8)	–	0.275(5)
	155	−8.93(2)	35.1(2)	0.518(1)	0.509(2)	0.748(4)	–	0.289(2)	1.289(1)	2.790(3)	2.579(8)	–	0.276(4)
	225	−8.10(2)	33.8(2)	0.489(1)	0.511(2)	0.722(5)	–	0.291(2)	1.251(1)	2.721(2)	2.483(7)	–	0.261(4)
	295	−7.51(2)	32.2(2)	0.460(1)	0.502(3)	0.704(7)	–	0.306(3)	1.213(1)	2.636(3)	2.368(7)	–	0.263(4)
0.75	85	−6.92(1)	32.3(2)	0.539(1)	0.533(1)	0.773(3)	–	0.278(2)	1.297(2)	2.797(4)	2.61(1)	–	0.256(5)
	155	−6.64(2)	30.9(2)	0.521(1)	0.533(2)	0.766(4)	–	0.289(1)	1.267(3)	2.772(4)	2.57(1)	–	0.261(6)
	225	−6.24(1)	29.3(2)	0.495(1)	0.527(2)	0.733(6)	–	0.293(2)	1.241(3)	2.686(4)	2.36(1)	–	0.251(5)
	295	−5.91(2)	27.9(2)	0.466(1)	0.509(3)	0.687(9)	–	0.309(3)	1.166(3)	2.564(4)	2.17(1)	–	0.28(1)
1.00	85	−5.91(2)	38.1(3)	0.550(1)	0.525(2)	0.791(5)	–	0.289(6)	1.309(2)	2.728(5)	2.49(1)	–	0.257(7)
	155	−3.07(1)	35.2(3)	0.524(1)	0.534(3)	0.775(6)	–	0.288(3)	1.261(2)	2.680(5)	2.45(1)	–	0.249(6)
	225	−2.90(1)	33.4(4)	0.499(1)	0.511(4)	0.71(1)	–	0.300(5)	1.201(7)	2.56(1)	2.23(2)	–	0.271(9)
	295	−2.74(1)	34.5(6)	0.476(1)	0.455(8)	0.63(1)	–	0.317(7)	1.113(5)	2.3†	2.1†	–	0.33(1)

* Relative to room temperature α-iron foil.
† Constrained value.

TABLE 6. Parameters obtained from the temperature dependence of the Mössbauer spectra of $Na_2(Mn_{1-x}Fe^{2+}_x)_2Fe^{3+}(PO_4)_3$

x	0.00	0.25	0.50	0.75	1.00
θ_M, tot. (K)	420(20)	430(8)	317(7)	395(4)	391(4)
M1 site					
$10^4 \times d\delta/dT$ Fe^{2+} [(mm/s)/K]	–	–	–	−7(1)	−8.2(4)
δ(0) Fe^{2+} (mm/s)	–	–	–	1.45(2)	1.456(8)
$\Delta E_{Q,2\text{-}2\text{-}3}(0)$ (mm/s)	–	–	–	3.05*	3.06*
$\Delta_{2\text{-}2\text{-}3}$ (cm^{-1})	–	–	–	620(33)	554(30)
$\Delta E_{Q,3\text{-}2\text{-}3}(0)$ (mm/s)	–	–	–	2.76*	2.74*
$\Delta_{3\text{-}2\text{-}3}$ (cm^{-1})	–	–	–	660(43)	558(35)
M2 site					
$10^4 \times d\delta/dT$ Fe^{2+} [(mm/s)/K]	−7.2(6)	−5.3(6)	−4.8(4)	−6(1)	−9.2(9)
$10^4 \times d\delta/dT$ Fe^{3+} [(mm/s)/K]	−4.9(4)	−4.1(5)	−3.7(2)	−3.5(2)	−3.53(6)
δ(0) Fe^{2+} (mm/s)	1.39(1)	1.37(1)	1.359(7)	1.36(2)	1.39(1)
δ(0) Fe^{3+} (mm/s)	0.578(9)	0.574(9)	0.573(5)	0.573(5)	0.579(1)
$\Delta E_{Q,2\text{-}3}(0)$ (mm/s)	–	2.9*	2.84*	2.8*	2.73*
$\Delta_{2\text{-}3}$ (cm^{-1})	–	694(30)	733(31)	708(15)	585(5)
$\Delta E_{Q,2\text{-}2}(0)$ (mm/s)	–	2.64*	2.64*	2.6*	2.48*
$\Delta_{2\text{-}2}$ (cm^{-1})	–	459(47)	656(24)	561(12)	566(19)
$\Delta E_{Q,2\text{-}Mn}(0)$ (mm/s)	2.78*	2.7*	–	–	–
$\Delta_{2\text{-}Mn}$ (cm^{-1})	663(40)	717(19)	–	–	–

* Parameter constrained to the value given.

TABLE 7. Wet chemical analyses of the synthetic alluaudite-type compounds, $Na_2(Mn_{1-x}Fe^{2+}_x)_2Fe^{3+}(PO_4)_3$

x	0.00	0.25	0.50	0.75	1.00
P_2O_5	41.46	41.38	42.52	41.57	41.86
Fe_2O_3*	12.85	19.50	20.38	21.28	19.76
FeO*	2.21	3.74	10.27	16.08	24.89
MnO	27.66	20.61	13.52	6.41	0.00
Na_2O	11.90	11.89	12.44	12.21	12.40
Total	96.08	97.12	99.13	97.55	98.91
Cation numbers					
P	3.000	3.000	3.000	3.000	3.000
Fe^{3+}	0.827	1.257	1.278	1.365	1.259
Fe^{2+}	0.158	0.268	0.716	1.146	1.762
Mn	2.002	1.495	0.954	0.463	0.000
Na	1.972	1.974	2.010	2.018	2.035

Note: The cation numbers were calculated on the basis of 3 P per formula unit.
* The Fe_2O_3 and FeO contents were calculated from the Fe^{3+}/Fe^{2+} ratios measured from the Mössbauer spectra.

To confirm the presence of vacancies, wet chemical analyses were performed (Table 7), which unexpectedly show a sodium content in good agreement with the nominal compositions. The difference between the data deduced from the X-ray structure refinements and the chemical compositions could indicate the presence of small amounts of impurities that were not detected by X-ray diffraction and Mössbauer spectroscopy. Maricite-type phosphates, for example, are Na-rich phases that have been identified in association with alluaudite in hydrothermal experiments at 400 to 800 °C (Hatert 2002a).

The M2 Fe^{3+} isomer shifts of the $Na_2(Mn_{1-x}Fe^{2+}_x)_2Fe^{3+}(PO_4)_3$ alluaudite-type compounds show a significant increase when x increases. This behavior is due to the decrease of the unit-cell volume when Mn^{2+} is replaced by Fe^{2+}. The excellent linear correlation between the unit-cell volume and the M2 Fe^{3+} isomer shifts is shown on Figure 12.

The alluaudite-type compounds $Na_2Mn_2Fe^{3+}(PO_4)_3$ ($x = 0.00$) and $Na_2MnFe^{2+}Fe^{3+}(PO_4)_3$ ($x = 0.50$) have previously been synthesized by Hatert et al. (2004), who reported Mössbauer measurements between 4.2 and 295 K. However, it must be stressed that the synthesis conditions used for these samples are very different from those used in the present study. $Na_2Mn_2Fe^{3+}(PO_4)_3$ was obtained through a solid state reaction in air, at 850 °C, and $Na_2MnFe^{2+}Fe^{3+}(PO_4)_3$ was hydrothermally synthesized at 700 °C and 3.5 kbar (Hatert et al. 2004). For this reason, the parameters obtained from the Mössbauer spectra are slightly different in the two papers. For example, $Na_2Mn_2Fe^{3+}(PO_4)_3$ obtained through the solid state reaction does not contain any trace of Fe^{2+} (Hatert et al. 2004), although the same compound synthesized by hydrothermal technique shows ca. 8 at% of Fe^{2+}. This difference is due to the very high oxygen fugacity which prevailed during the solid state synthesis in air as compared to the lower oxygen

M1 Fe^{2+} (mm/s)			
δ*	$\Delta E_{Q,2\text{-}2\text{-}3}$	$\Delta E_{Q,3\text{-}2\text{-}3}$	Γ
–	–	–	–
–	–	–	–
–	–	–	–
–	–	–	–
–	–	–	–
–	–	–	–
–	–	–	–
–	–	–	–
–	–	–	–
–	–	–	–
–	–	–	–
–	–	–	–
1.387(3)	3.035(8)	2.754(8)	0.271(8)
1.366(6)	2.92(1)	2.652(6)	0.271(8)
1.288(4)	2.84(1)	2.579(6)	0.259(8)
1.258(4)	2.68(1)	2.498(8)	0.238(9)
1.382(2)	3.060(5)	2.74(1)	0.303(6)
1.335(3)	2.902(7)	2.567(8)	0.306(6)
1.272(6)	2.73(1)	2.465(8)	0.285(9)
1.211(2)	2.591(5)	2.325(7)	0.249(6)

fugacity prevailing during the hydrothermal synthesis.

An important difference between the results given by Hatert et al. (2004) and herein is the assignment of ΔE_Q Fe^{3+} for $Na_2Mn_2Fe^{3+}(PO_4)_3$. The values of $\Delta E_{Q,3\text{-}Mn}$ reported by Hatert et al. (2004) are larger than the values of $\Delta E_{Q,3\text{-}3}$, an observation which can be explained by the significant distortion affecting the adjacent M2 octahedra when they are occupied by Fe^{3+} and Mn^{2+}. In contrast, the values of $\Delta E_{Q,3\text{-}Mn}$ given herein are smaller than the values of $\Delta E_{Q,3\text{-}3}$. The reason for this difference is unknown, but another model with an assignment similar to that proposed by Hatert et al. (2004) was undertaken. The fits obtained with this model were very poor, and it was decided to retain the first model even in view of the different values of $\Delta E_{Q,3\text{-}Mn}$ and $\Delta E_{Q,3\text{-}3}$.

Because Fe^{2+} occurs at both the M1 and M2 crystallographic sites, it is possible to compare the values of isomer shifts and quadrupole splittings of these sites. The quadrupole splittings and isomer shifts of Fe^{2+} at the M1 site are larger than those of Fe^{2+} at the M2 site (Table 5), thus indicating that the M1 site is larger and more distorted than M2. These observations corroborate the structural data previously reported in the literature (Moore 1971; Hatert et al. 2000).

Acknowledgments

Many thanks to two anonymous reviewers for their constructive comments concerning this manuscript. G.J..L thanks the Francqui Foundation for his appointment as "Chaire Francqui Interuniversitaire au Titre étranger" during the 2002–2003 academic year. FH acknowledges the Fonds National de la Recherche Scientifique, Belgium, for his nomination as "Chargé de Recherches" (Postdoctoral Researcher). The authors also acknowledge the financial support of the Fonds National de la Recherche Scientifique, Belgium, for grant 9.4565.95, and of the "Région Wallone", for grant RW/115012 NOMADE.

References cited

Antenucci, D. (1992) Synthèse et cristallochimie de composés à structure alluaudite. Incidences dans les processus d'altération des phosphates Fe-Mn des pegmatites granitiques, 259 p. Unpublished Ph.D. Thesis, University of Liège.

Antenucci, D., Miehe, G., Tarte, P., Schmahl, W.W., and Fransolet, A.-M. (1993) Combined X-ray Rietveld, infrared and Raman study of a new synthetic variety of alluaudite, $NaCdIn_2(PO_4)_3$. European Journal of Mineralogy, 5, 207–213.

Antenucci, D., Fransolet, A.-M., Miehe, G., and Tarte, P. (1995) Synthèse et cristallochimie de $NaCaCdMg_2(PO_4)_3$, phosphate nouveau à structure alluaudite sans cation trivalent. European Journal of Mineralogy, 7, 175–181.

Ben Smail, R. and Jouini, T. (2002) $AgNi_3(PO_4)(HPO_4)_2$: an alluaudite-like structure. Acta Crystallographica, C58, i61–i62.

Burnham, C.W. (1991) LCLSQ version 8.4, least-squares refinement of crystallographic lattice parameters. Department of Earth and Planetary Sciences, Harvard University.

Černý, P. (1991) Rare-element granitic pegmatites. Part I: Anatomy and internal evolution of pegmatite deposits. Geoscience Canada, 18, 49–67.

Chouaibi, N., Daidouh, A., Pico, C., Santrich, A., and Veiga, M.L. (2001) Neutron diffraction, Mössbauer spectrum, and magnetic behavior of $Ag_2FeMn_2(PO_4)_3$ with alluaudite-like structure. Journal of Solid State Chemistry, 159, 46–50.

Corbin, D.R., Whitney, J.F., Fultz, W.C., Stucky, G.D., Eddy, M.M., and Cheetham, A.K. (1986) Synthesis of open-framework transition-metal phosphates using organometallic precursors in acidic media. Preparation and structural characterization of $Fe_3P_4O_{20}H_{10}$ and $NaFe_3P_3O_{12}$. Inorganic Chemistry, 25, 2279–2280.

Daidouh, A., Durio, C., Pico, C., Veiga, M.L., Chouaibi, N., and Ouassini, A. (2002) Structural and electrical study of the alluaudites $(Ag_{1-x}Na_x)_2FeMn_2(PO_4)_3$ (x = 0, 0.5 and 1). Solid State Sciences, 4, 541–548.

Durio, C., Daidouh, A., Chouaibi, N., Pico, C., and Veiga, M.L. (2002) Electrical behavior of new orthophosphates $Na_2M_3(PO_4)_3$ (M_3 = $GaMn_2$, $GaCd_2$, $InMn_2$ and FeMnCd) with alluaudite-like structure. Journal of Solid State Chemistry, 168, 208–216.

Farmer, V.C. (1974) The infrared spectra of minerals. Mineralogical Society Monographs, 4, 539.

Fransolet, A.-M., Abraham, K., and Speetjens, J.-M. (1985) Evolution génétique et signification des associations de phosphates de la pegmatite d'Angarf-Sud, plaine de Tazenakht, Anti-Atlas, Maroc. Bulletin de Minéralogie, 108, 551–574.

Fransolet, A.-M., Keller, P., and Fontan, F. (1986) The phosphate mineral associations of the Tsaobismund pegmatite, Namibia. Contributions to Mineralogy and Petrology, 92, 502–517.

Guesmi, A. and Driss, A. (2002) $AgCo_3PO_4(HPO_4)_2$. Acta Crystallographica, C58, i16-i17.

Hartmann-Boutron, F. and Imbert, P. (1968) Mössbauer study of the electronic and magnetic properties of Fe^{2+} done in some spinel-type compounds. Journal of Applied Physics, 39, 775–784.

Hatert, F. (2002a) Cristallochimie et synthèse hydrothermale d'alluaudites dans le système Na-Mn-Fe-P-O: contribution au problème de la genèse de ces phosphates dans les pegmatites granitiques. Unpublished Ph.D. Thesis, University of Liège, 247 p.

——— (2002b) The stability of alluaudite in granitic pegmatites: a study of the $Na_2(Mn_{1-x}Fe^{2+}_x)_2Fe^{3+}(PO_4)_3$ solid solution. Abstract book, 18th General Meeting of the International Mineralogical Association, Edinburgh, 91.

Hatert, F. and Fransolet, A.-M. (2002). Stability of the alluaudite + triphylite paragenesis in granitic pegmatites. Abstract book, 18th General Meeting of the International Mineralogical Association, Edinburgh, 209.

Hatert, F., Keller, P., Lissner, F., Antenucci, D., and Fransolet, A.-M. (2000) First experimental evidence of alluaudite-like phosphates with high Li-content: the $(Na_{1-x}Li_x)MnFe_2(PO_4)_3$ series (x = 0 to 1). European Journal of Mineralogy, 12, 847–857.

Hatert, F., Antenucci, D., Fransolet, A.-M., and Liégeois-Duyckaerts, M. (2002) The crystal chemistry of lithium in the alluaudite structure: a study of the $(Na_{1-x}Li_x)CdIn_2(PO_4)_3$ solid solution (x = 0 to 1). Journal of Solid State Chemistry, 163, 194–201.

Hatert, F., Hermann, R.P., Long, G.J., Fransolet, A.-M., and Grandjean, F. (2003) An X-ray Rietveld, infrared, and Mössbauer spectral study of the $NaMn(Fe_{1-x}In_x)_2(PO_4)_3$ alluaudite-type solid solution. American Mineralogist, 88, 211–222.

Hatert, F., Long, G.J., Hautot, D., Fransolet, A.-M., Delwiche, J., Hubin-Franskin, M.J., and Grandjean, F. (2004) A structural, magnetic, and Mössbauer spectral study of several Na-Mn-Fe-bearing alluaudites. Physics and Chemistry of Minerals, 31, 487–506.

Herber, R.H. (1984) Structure, bonding, and the Mössbauer lattice temperature. In R.H. Herber, Ed., Chemical Mössbauer Spectroscopy, p. 199. Plenum Press, New York.

Hermann, R.P., Hatert, F., Fransolet, A.-M., Long, G.J., and Grandjean, F. (2002) Mössbauer spectral evidence for next-nearest neighbor interactions within the alluaudite structure of $Na_{1-x}Li_xMnFe_2(PO_4)_3$. Solid State Sciences, 4, 507–513.

Hidouri, M., Lajmi, B., Driss, A., and Ben Amara, M. (2003) The alluaudite-like phosphate $Na_{1.79}Mg_{1.79}Fe_{1.21}(PO_4)_3$. Acta Crystallographica, E59, i7–i9.

Ingalls, R. (1964) Electric-Field Gradient Tensor in Ferrous Compounds. Physical Review, 133, A787–A795.

Korzenski, M.B., Schimek, G.L., Kolis, J.W., and Long, G.J. (1998) Hydrothermal synthesis, structure, and characterization of a mixed-valent iron (II/III) phosphate, $NaFe_{3.67}(PO_4)_3$: a new variation of the alluaudite structure type. Journal

of Solid State Chemistry, 139, 152–160.

Leroux, F., Mar, A., Payen, C., Guyomard, D., Verbaere, A., and Piffard, Y. (1995a) Synthesis and structure of $NaMn_3(PO_4)(HPO_4)_2$, an unoxidized variant of the alluaudite structure type. Journal of Solid State Chemistry, 115, 240–246.

Leroux, F., Mar, A., Guyomard, D., and Piffard, Y. (1995b) Cation substitution in the alluaudite structure type : synthesis and structure of $AgMn_3(PO_4)(HPO_4)_2$. Journal of Solid State Chemistry, 117, 206–212.

Lii, K.H. and Shih, P.F. (1994) Hydrothermal synthesis and crystal structures of $NaCo_3(PO_4)(HPO_4)_2$ and $NaCo_3(AsO_4)(HAsO_4)_2$: synthetic modifications of the mineral alluaudite. Inorganic Chemistry, 33, 3028–3031.

Lii, K.-H. and Ye, J. (1997) Hydrothermal synthesis and structure of $Na_3In_2(PO_4)_3$ and $Na_3In_2(AsO_4)_3$: synthetic modifications of the mineral alluaudite. Journal of Solid State Chemistry, 131, 131–137.

Moore, P.B. (1971) Crystal chemistry of the alluaudite structure type: Contribution to the paragenesis of pegmatite phosphate giant crystals. American Mineralogist, 56, 1955–1975.

Rulmont, A., Cahay, R., Liégeois-Duyckaerts, M., and Tarte, P. (1991) Vibrational spectroscopy of phosphates: some general correlations between structure and spectra. European Journal of Solid State and Inorganic Chemistry, 28, 207–219.

Shannon, R.D. (1976) Revised effective ionic radii and systematic studies of interatomic distances in halides and chalcogenides. Acta Crystallographica, A32, 751–767.

Tuttle, O.F. (1949) Two pressure vessels for silicate-water studies. Geological Society of America Bulletin, 60, 1727–1729.

Vandenberghe, R.E. and De Grave, E. (1989) Mössbauer effect studies of oxidic spinels. In G.J. Long and F. Grandjean, Eds., Mössbauer Spectroscopy Applied to Inorganic Chemistry, 3, 59–182. Plenum Press, New York.

Warner, T.E., Milius, W., and Maier, J. (1993) Synthesis and structure of $Cu_{1.35}Fe_3(PO_4)_3$ and $Cu_2Mg_3(PO_4)_3$: new mixed valence compounds of the alluaudite structure type. Journal of Solid State Chemistry, 106, 301–309.

White, B.W. and Keramidas, V.G. (1972) Vibrational spectra of oxides with the *C*-type rare earth oxide structure. Spectrochimica Acta, 28A, 501–509.

Yakubovich, O.V., Simonov, M.A., Egorov-Tismenko, Y.K., and Belov, N.V. (1977) The crystal structure of a synthetic variety of alluaudite, $Na_2(Fe^{3+}_{0.5}Fe^{2+}_{0.5})_2Fe^{2+}[PO_4]_3$. Soviet Physics Doklady, 22, 550–552.

Young, R.A., Larson, A.C., and Paiva-Santos, C.O. (1998) User's guide to program DBWS-9807 for Rietveld analysis of X-ray and neutron powder diffraction patterns, 56 p. School of Physics, Georgia Institute of Technology, Atlanta, U.S.A.

MANUSCRIPT RECEIVED NOVEMBER 18, 2003
MANUSCRIPT ACCEPTED AUGUST 31, 2004
MANUSCRIPT HANDLED BY PETER BURNS